N90-12518

EFFECT OF ROUGHNESS ON THE STABILITY OF BOUNDARY LAYERS

Ali H. Nayfeh, Saad A. Ragab, and Ayman Al-Maaitah
Department of Engineering Science and Mechanics
Virginia Polytechnic Institute and State University
Blacksburg, Virginia

The instability of flows around hump and dip imperfections is investigated. The mean flow is calculated using interacting boundary layers, thereby accounting for viscous/inviscid interaction and separation bubbles. Then, the two-dimensional linear instability of this flow is analyzed, and the amplification factors are computed. Results are obtained for several height/width ratios and locations. The theoretical results have been used to correlate the experimental results of Walker and Greening.[1] The observed transition locations are found to correspond to amplification factors varying between 7.4 and 10, consistent with previous results for flat plates. The method accounts for Tollmien-Schlichting waves, the shear layer instability, and their interaction. Separation is found to significantly increase the amplification factor.

1. INTRODUCTION

The performance of natural laminar flow (NLF) airfoils is critically dependent on the location of transition, which may be strongly influenced by surface imperfections. Although modern metal and composite manufacturing techniques can provide smooth surfaces that are compatible with NLF, manufacturing tolerance criteria are needed for other unavoidable surface imperfections. These imperfections include waviness and bulges, steps and gaps at junctions, and three-dimensional roughness elements such as flush screw head slots and incorrectly installed flush rivets. Other unavoidable discontinuities arise from the installation of leading edge panels on wings, nacelles, and empennage surfaces and the installation of access panels, doors, and windows on fuselage noses and engine nacelles[2-4]. Because discontinuities cannot be avoided, a guide is needed for manufacturing tolerances. The guide is not related to the drag generated by these discontinuities, but it is related to their allowable sizes so that laminar flow can be maintained. The mechanisms by which these imperfections cause transition include amplification of Tollmien-Schlichting waves, Kelvin-Helmholtz instability (for separated flows), amplification of crossflow vorticity, Gortler instability, enhancement of receptivity of freestream turbulence and acoustic disturbances, and any interaction between two or more of these mechanisms[4-9].

Walker and Greening[1] made wind tunnel experiments to determine the effect of two-dimensional smooth bulges and hollows on the transition of the flow over a flat plate. They used surface tubes to determine the location of transition from laminar to turbulent flow. Their bulges and hollows were mounted on one side of a smooth flat aluminum plate, having an elliptic leading edge. Hislop[10] carried out similar experiments for narrow spanwise surface ridge corrugations on a flat plate. Walker and Cox[11] made wind tunnel experiments to study the effect of spanwise corrugations on an airfoil. These experiments were made for three forms of narrow corrugations (flat, arch and wire) situated in the laminar boundary layer of a large symmetric airfoil (EQH 1260 section), mounted at zero angle of attack.

Fage[5] collected the three previous works[1,10-11] and established criteria for the critical heights of these imperfections that cause transition from laminar to turbulent flow. He found out that the flow conditions near a corrugation which affect transition are associated with a separation of the laminar boundary layer from its surface. Carmichael[6-8] also developed empirically based criteria for allowable waviness and roughnesses that cause either laminar separation or amplification of Tollmien-Schlichting waves. His criteria are for allowable single and multiple bulges or sinusoidal waviness for both swept and unswept wing surfaces. His experiments include the influence of compressibility, suction, pressure gradients, multiple imperfections, and wing sweep. The flight experiments of Holmes, Obara, Martin and Domack[4] demonstrate the strong influence of shapes of steps on the transition location and hence on the allowable heights of such imperfections. They found that by rounding a foward-facing step, the transition Reynolds number increases from 1800 to 2700. Carmichael's criteria are based on experimental results for waves located more than 25-percent chord downstream of the leading edge and hence they will underpredict allowable imperfections in the leading edge region and overpredict allowable imperfections in regions of unaccelerated flows. Klebanoff and Tidstrom[12] used a spanwise trip wire as a roughness element, which causes local upstream and downstream separations, the latter extending forty to fifty times the height of the wire before reattachment to the wall.

Inspite of all these investigations, an understanding of the physics of the instability of flows around surface imperfections is still lacking. As a first step toward such an understanding, this work investigates the influence of a two-dimensional hump or dip on the two-dimensional stability. This work uses a combination of linear stability theory and the exp(N) criterion that has proven to be a valuable tool for correlating transition and for evaluating natural laminar flow as well as laminar flow control concepts. Since linear stability of parallel as well as nonparallel incompressible and compressible flows is well established, the major task in evaluating the influence of imperfections is an accurate prediction of the mean flow.

For smooth surfaces, one can use a conventional boundary-layer formulation to solve for the mean flow over swept and unswept wing surfaces. However, conventional boundary-layer formulations cannot predict flow over surfaces with imperfections, such as suction strips and slots, waviness and bulges, steps and gaps at junctions, and three-dimensional roughness elements because of the strong viscous/inviscid coupling and flow separation. Instead, one needs to use a triple-deck formulation, an interacting boundary-layer formulation, or a Navier-Stokes solver. All these approaches account for the viscous/inviscid interaction as well as separation bubbles, but Navier-Stokes solvers are very expensive compared with triple-deck and interacting boundary-layer formulations. In this work, we use an interacting boundary-layer formulation, which already had been used to compute compressible as well as incompressible flows over smooth steps, wavy surfaces and humps, convex and concave corners, suction or blowing slots, and finite-angle trailing edges. In most of these applications separation bubbles and upstream influence exist and comparisons with solutions of the Navier-

Stokes equations and/or experiments had shown good agreement. Gleyzes, Cousteix and Bonnet[13], Vatsa and Carter[14], and Davis and Carter[15] used interacting boundary-layer theory to analyze separation bubbles near the leading edges of airfoils. Davis, Carter and Reshotko[16] developed an interacting boundary-layer technique for the calculation of transitional separation bubbles over infinite swept wings; the results are in good agreement with Horton's[17] detailed experimental data for separated flow over a swept plate.

The purpose of this work is to study the effect of a two-dimensional roughness element or a two-dimensional surface waviness, represented by a hump or a dip, on the two-dimensional stability of boundary layers over flat plates. Quartic humps with different sizes and locations are studied first. Then, the theory is used to correlate the experimental data of Walker and Greening.

2. MEAN FLOW

The two-dimensional incompressible laminar boundary layer over the plate and the hump is determined by solving the interacting boundary-layer equations[18,19]. These equations account for upstream influence through the interaction of the viscous flow with the inviscid flow outside the boundary layer. Moreover, they are also capable of capturing separation bubbles without difficulties. Solutions are obtained by using a finite-difference method in which the grid spacings acknowledge the scalings predicted by the triple-deck theory in the interaction region.

Figure 1 shows a small symmetric hump of height h^* and width $2b^*$ whose center is located at x_m^*. We introduce dimensionless variables using L^* and U^*, where L^* is the distance from the leading edge to a reference point, and ∞ reference quantities. In terms of dimensionless variables, the hump shape is given by

$$y = \frac{y^*}{L^*} = \frac{h^*}{L^*} f(\zeta) \tag{1}$$

where

$$\zeta = \frac{x^* - x_m^*}{b^*} = \frac{x - x_m}{b} \tag{2}$$

We present numerical results for a quadratic hump given by

$$f(\zeta) = \begin{cases} (1 - \zeta^2)^2 & \text{if } |\zeta| \le 1 \\ 0 & \text{if } |\zeta| > 1 \end{cases} \tag{3}$$

and the Walker and Greening hump

$$f(\zeta) = \begin{cases} 1 - 3\zeta^2 + 2|\zeta|^3 & \text{if } |\zeta| \le 1 \\ 0 & \text{if } |\zeta| > 1 \end{cases} \tag{4}$$

Figure 2 shows the variation of the height of a hump, corresponding to h = 3 in triple-deck variables, and the resulting displacement thickness. Figure 3 shows the distributions of the skin friction and pressure coefficients for the hump shown in Fig. 2. A small separation bubble is formed on the lee side of the hump.

Tables 1 and 2 show some of the mean-flow properties for the humps and dips of Walker and Greening. The velocity u outside the boundary layer for the undistorted surface varies from 15.9 m/sec (53.0 ft/sec) to 28.5 m/sec (95.0 ft/sec) for the humps, and from 18.57 m/sec (61.9 ft/sec) to 25.47 m/sec (84.9 ft/sec) for the dips. The maximum transverse dimension h* varies from 0.75 mm (0.03 in) to 1.75 mm (0.07 in) for the humps and from 1.425 mm (0.057 in) to 1.675 mm (0.067 in) for the dips. The observed transition length is denoted by L_T; it is measured from the leading edge to the observed transition location. The Reynolds numbers at the middle of the humps or dips R_m and at the transition location R_T are based on the reference length δ^* so that

$$R_m = (Re)^{\frac{1}{2}}, \quad R_T = \left(\frac{L_T}{L}\frac{}{\delta^*} Re\right)^{\frac{1}{2}} \tag{5}$$

All of the previous quantities were calculated directly from the experimental data given by Walker and Greening, but the streamwise extents of the separation bubbles are expressed as the difference in the Reynolds numbers at separation and reattachment; that is, ΔR = R(reattachment) - R(separation) and ΔR is calculated using the interacting boundary-layer code. Except for hump No. 1 all the humps and dips in Tables 1 and 2 have separation bubbles.

Figure 4 shows the variation of the streamwise velocity profiles for hump No. 14. The first and the last velocity profiles are at locations away from the hump; they are essentially Blasius profiles.

3. STABILITY ANALYSIS

We consider the two-dimensional spatial quasi-parallel stability of the basic state determined by the interacting boundary-layer code. To this end, we superimpose on it a two-dimensional unsteady disturbance. Thus, we let

$$\tilde{q}(x,y,t) = Q(y) + \hat{q}(x,y,t) \tag{6}$$

where q refers to the pressure p and the velocity components u and v in the streamwise direction x and the transverse direction y, respectively. Substituting the assumed flow into the Navier-Stokes equations, subtracting the basic-flow quantities, and linearizing the resulting equations, we obtain equations describing the disturbance. We consider the case of spatial stability and determine the amplification rate $-\alpha_i$, where α_i is the imaginary part of the complex wavenumber α.

For a given U, ω, and R, we determine α and then calculate the N factor from

$$N = -2\int_{R_0}^{R} \alpha_i dR \tag{7}$$

where R_θ is the Reynolds number corresponding to branch I of the neutral stability curve.

Figure 5 shows the variation of the growth rate with streamwise distance for the hump shown in Fig. 2. Shown also is the growth rate of the Blasius flow at the same frequency. The presence of the hump first increases the growth rate then it decreases the growth rate and finally increases the growth rate again. The stabilizing and destabilizing effects are consistent with the gradients of the pressure distributions shown in Fig. 3.

The amplification of two-dimensional disturbances is the result of a complex interaction of Tollmien-Schlichting waves and shear-layer (laminar separation) instability as evident from Figs. 4 and 6. They show the variation of the streamwise velocity profile and the corresponding eigenfunction of the instability wave, respectively, with distance along the plate. Ahead of the separation region, the eigenfunction has a character typical of T-S waves with two peaks, a large one at the critical layer and a small peak near the edge of the boundary layer. In the separation region, the eigenfunctions develop a third peak at the inflection point of the mean-flow profile. This peak increases with distance from the separation point, achieves a maximum which can be comparable to the peak at the critical layer, and decreases to zero at the reattachment point. The effects of the shear-layer instability are to increase the growth rates and the dangerous frequency.

Table 3 shows the variations of the Reynolds number R_θ at which N = 9 and the computed amplification factor N_T at the experimentally measured transition location with the dimensionless frequency F for hump No. 5 in Table 1. For $F = 45\times10^{-6}$, the maximum value of N is 8.4. It is clear that the most dangerous frequency has shifted from $F = 25\times10^{-6}$ for the Blasius flow to $F = 37.5\times10^{-6}$ for the disturbed flow. Moreover, the maximum computed amplification factor at the experimental transition location is 8.7.

Tables 4 and 5 summarize the computed results for all the hump and dip configurations of Walker and Greening. They show the maximum (maximized over all frequencies) amplification factor N_T and its corresponding frequency at the measured transition location. The values of N_T range from 7.4 to 10, consistent with previous results for flat plates.

4. CONCLUSIONS AND RECOMMENDATIONS

An analysis is conducted of the effect of imperfections consisting of humps and dips on the stability of incompressible flows over flat plates. The mean flow is calculated using interacting boundary layers. Linear quasiparallel spatial stability is used to calculate the growth rates and mode shapes of two-dimensional disturbances. Then, the amplification factor is computed. A search for the most dangerous frequency is conducted based on an amplification factor of 9 in the shortest distance. Correlations are made with the transition experiment of Walker and Greening using the e^9 method.

Based on the present investigations, it can be concluded that:

1. The e^9 method gives a good estimate of the transition location.

2. Increasing the size of the separation bubble, by increasing either the height-to-width ratio or the freestream Reynolds number, causes transition to occur sooner.

3. In the separation bubble, the calculated growth rates of the disturbances account for both the T-S and shear-layer instabilities.

4. The shape of a smooth hump or dip does not have a significant effect on the growth rates.

5. The geometrical factors of the imperfection that govern the instability are:

   a. the height-to-width ratio.

   b. the location of the imperfection element from the leading edge of the plate and Branch I of the Blasius stability curve.

6. The most dangerous frequency in the presence of the roughness element is not the same as that for the Blasius flow.

The present study needs to be extended by accounting for:

a. nonlinear effects (in view of the large growth rates encountered in separation regions).

b. nonparallel effects.

c. the effects of concave curvature (i.e., Görtler instability).

d. the receptivity to acoustic and free-stream disturbances.

e. the interaction between any of the instability mechanisms.

More experiments need to be conducted to provide detailed measurements of the mean profiles, mode shapes, growth rates, etc. that can be used to corroborate the theoretical results.

ACKNOWLEDGMENT

This work was supported by the United States Office of Naval Research under Contract No. N00014-85-K-0011, NR 4325201, and the National Aeronautics and Space Administration under Grant No. NAG-1-714.

REFERENCES

1. Walker, W. S.; and Greening, J. R.: Brit. A.R.C. 5950, 1942.

2. Holmes, B. J.; Obara, C. J.; and Yip, L. P.: NASA TP 2256, 1984.

3. Obara, C. J.; and Holmes, B. J.: NASA TP 2417, 1985.

4. Holmes, B. J.; Obara, C. J.; Martin, G. L.; and Domack, C. S.: presented at the 1985 SAE General Aviation Meeting and Exposition, Wichita, Kansas, SAE Paper No. 850863, 1985.

5. Fage, A.: Report and Memorandum No. 2120, Brit. A.R.C., 1943.

6. Carmichael, B. H.; Whites, R. C.; and Pfenninger, W.: Northrup Aircraft Inc. Rep. No. NAI-57-1163 (BLC-101), 1957.

7. Carmichael, B. H.: Norair Rep. No. NOR-59-438 (BLC-123), 1959.

8. Carmichael, B. H.; and Pfenninger, W.: "Surface Imperfection Experiments on a Swept Laminar Suction Wing", Norair Rep. No. NOR-59-454 (BLC-124), 1959.

9. Goldstein, M. E.: Journal of Fluid Mechanics, vol. 154, 1985, p. 509.

10. Hilsop, G. S.: Brit. A.R.C. 6443, 1943.

11. Walker, W. S.; and Cox, R. J.: Brit. A.R.C. 6126, 1942.

12. Klebanoff, P. S.; and Tidstrom, K. P.: Physics of Fluids, vol. 15, 1972, p. 1173.

13. Gleyzes, C.; Cousteix, J.; and Bonnet, J. L.: in Second Symposium on Numerical and Physical Aspects of Aerodynamic Flows, (Proceedings, Springer-Verlag, 1983).

14. Vatsa, V. N.; and Carter, J. E.: AIAA Journal, vol. 22, 1984, p. 1697.

15. Davis, R. L.; and Carter, J. E.: AIAA Journal, vol. 25, 1986, p. 850.

16. Davis, R. L.; Carter, J. E.; and Reshotko, E.: AIAA Journal, vol. 25, 1987, p. 421.

17. Horton, H. P.: Ph.D. Thesis, University of London, (Queen Mary College, 1968).

18. Davis, R. L.; and Werle, M. J.: "Progress on Interacting Boundary-Layer Computations atHigh Reynolds Number", in the Numerical and Physical Aspects of Aerodynamic Flows, (ed. T. Cebeci, Springer-Verlag, New York, 1982).

19. Ragab, S. A.; and Nayfeh, A. H.: "A Comparison of the Second-Order Triple-Deck Theory with Interacting Boundary Layers", in Numerical and Physical Aspects of Aerodynamic Flows, (ed. T. Cebeci, Springer-Verlag, New York, 1982).

Table 1. Hump configurations in the experiments of Walker and Greening

Number	u ft/sec	h in	L_T ft	h*/b*	R_m	R_T	Bubble size ΔR
1	82.6	0.031	4.58	0.0155	812	1346	00.0
2	69.4	0.0525	4.58	0.0263	830	1376	18.0
3	70.4	.0555	4.58	0.0278	860	1426	29.6
4	53.0	0.0620	4.58	0.0310	744	1234	25.7
5	56.2	0.0665	4.58	0.0332	764	1267	28.8
6	53.8	0.0700	4.58	0.0350	753	1249	36.1
7	78.0	0.0530	3.75	0.0265	904	1357	26.9
8	76.0	0.0555	3.75	0.0278	892	1337	32.5
9	61.5	0.0620	3.75	0.0310	803	1205	31.6
10	62.4	0.0630	3.75	0.0315	810	1215	34.5
11	55.5	0.0680	3.75	0.0340	761	1142	34.6
12	95.0	0.0525	2.92	0.0263	997	1319	32.6
13	70.0	0.0620	2.92	0.0310	860	1138	32.8
14	92.4	0.0620	2.08	0.0310	983	1098	49.9

Table 2. Dip configurations in the experiments of Walker and Greening

Number	u ft/sec	h in	L_T ft	h*/b*	R_m	R_T	Bubble size ΔR
1	76.4	-0.057	4.58	0.0285	894	1483	37.7
2	65.8	-0.067	4.58	0.0335	831	1377	41.6
3	82.7	-0.057	3.75	0.0285	930	1395	39.8
4	61.9	-0.067	3.75	0.0335	807	1210	36.5
5	84.9	-0.057	2.92	0.0285	943	1248	41.3
6	69.7	-0.067	2.92	0.0285	855	1132	39.0

Table 3. Variation of the maximum N-factor and the location at which N = 9 with the height of a quartic hump of half-width $\frac{b^*}{L^*_m} = 2.274\times10^{-2}$ $(\frac{b^*}{\delta} = 4.430)$ whose center is at $R_m = 975$: $\delta = 5\ \frac{\nu L^*}{U}$

$\frac{h^*}{L^*}$	$\frac{h^*}{\delta}$	$\frac{h^*}{b^*}$	R_9	N_{max}	Bubble length ΔR
0	0	0	1792	9.84	0
4.198×10^{-4}	0.082	0.019	1779	10.04	0
5.457×10^{-4}	0.106	0.024	1750	10.25	0
8.395×10^{-4}	0.164	0.037	1680	11.02	6.7
12.593×10^{-4}	0.246	0.055	1552	12.67	22.1

Table 4. Correlation of the theoretical and experimental results for the transition location for the humps in Table 1

Hump#	h^* in	$\frac{h^*}{b^*}$	R_m	Separation bubble ΔR	R_T	N_T	$F_T\times10^6$
1	0.0310	0.0155	812	00.0	1346	10.03	20.0
2	0.0525	0.0262	830	18.0	1376	8.20	37.5
3	0.0555	0.0278	860	29.6	1426	9.09	35.0
4	0.062	0.0319	744	25.7	1234	7.95	40.0
5	0.0665	0.0333	764	28.8	1267	8.70	37.5
6	0.0700	0.0350	753	36.1	1249	9.10	40.0
7	0.0530	0.0265	904	26.9	1356	8.30	37.5
8	0.0555	0.0278	892	32.5	1337	8.19	35.0
9	0.0620	0.0310	803	31.7	1205	7.90	45.0
10	0.0630	0.0315	810	34.5	1215	8.00	42.5
11	0.0680	0.0340	761	34.6	1142	7.85	45.0
12	0.0525	0.0263	997	32.0	1319	9.20	35.0
13	0.0620	0.0310	860	32.8	1138	7.40	45.0
14	0.0620	0.0310	983	49.9	1098	9.00	55.0

Table 5. Correlation of the theoretical and experimental results for the transition location for the dips in Table 2

Dip#	$-h^*$	$\frac{h^*}{b^*}$	R_m	Separation bubble ΔR	R_T	N_T	$F_T \times 10^6$
1	0.057	0.0285	894	37.7	1483	9.2	30
2	0.067	0.0335	831	41.6	1377	8.9	35
3	0.057	0.0285	930	39.8	1395	8.31	35
4	0.067	0.0335	807	36.5	1210	7.5	40
5	0.057	0.0285	943	41.3	1248	7.3	45
6	0.067	0.0335	855	39.0	1132	6.69	50

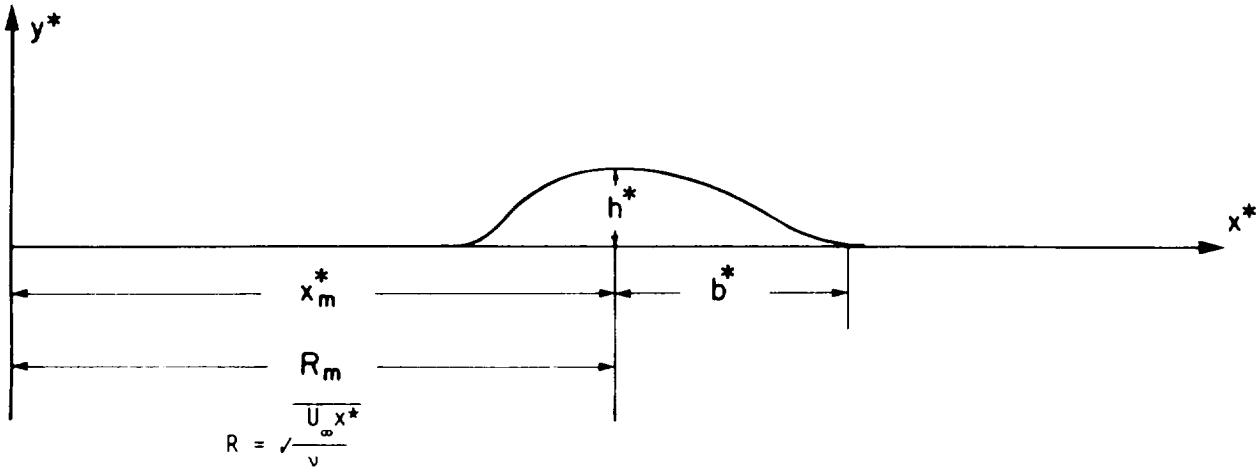

$$R = \sqrt{\frac{U_\infty x^*}{\nu}}$$

$$\frac{y^*}{h^*} = (1 - \zeta^2)^2 : \text{ Quartic}$$

$$\frac{y^*}{H^*} = 1 - 3\zeta^2 + 2|\zeta|^3 : \text{ Walker and Greening}$$

$$\zeta = \frac{x^* - x_m^*}{b^*}$$

* Height, Location, and Shape

Figure 1. Hump configuration.

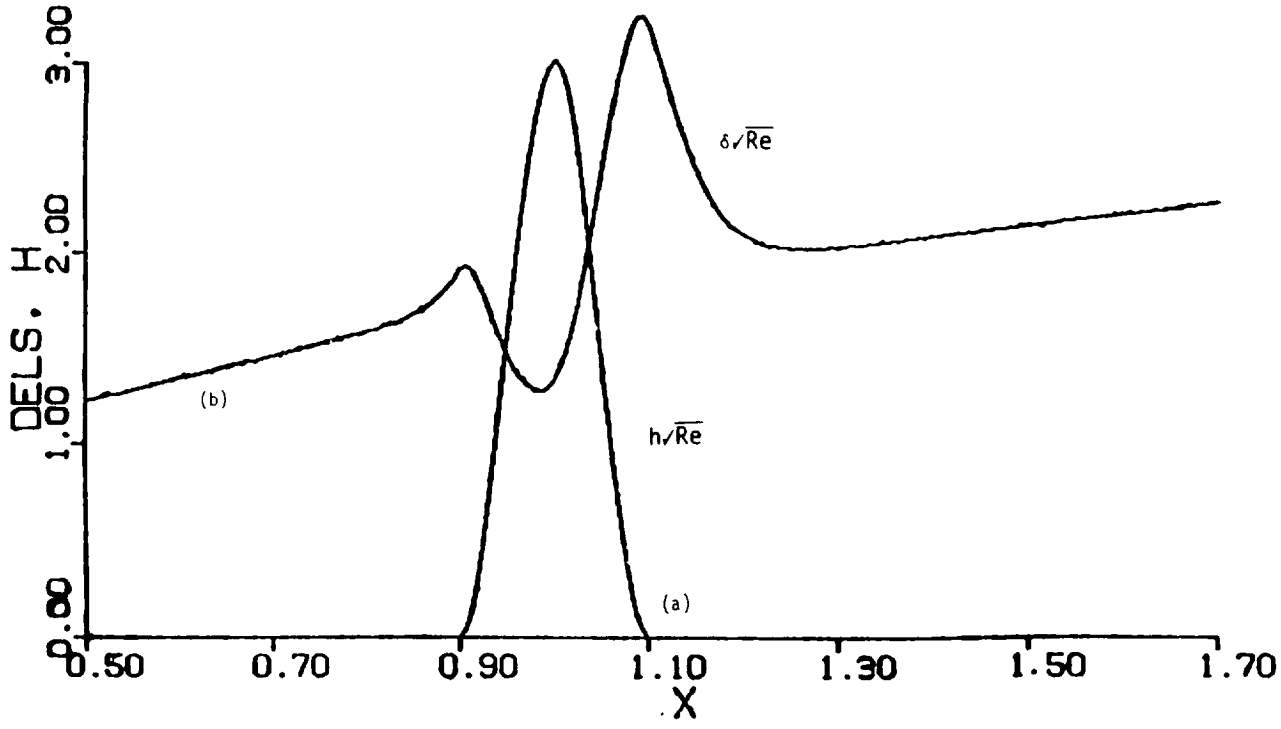

Figure 2. (a) Hump shape for h = 3, and
(b) corresponding displacement surface $\delta\sqrt{Re}$; Re = 10^6.

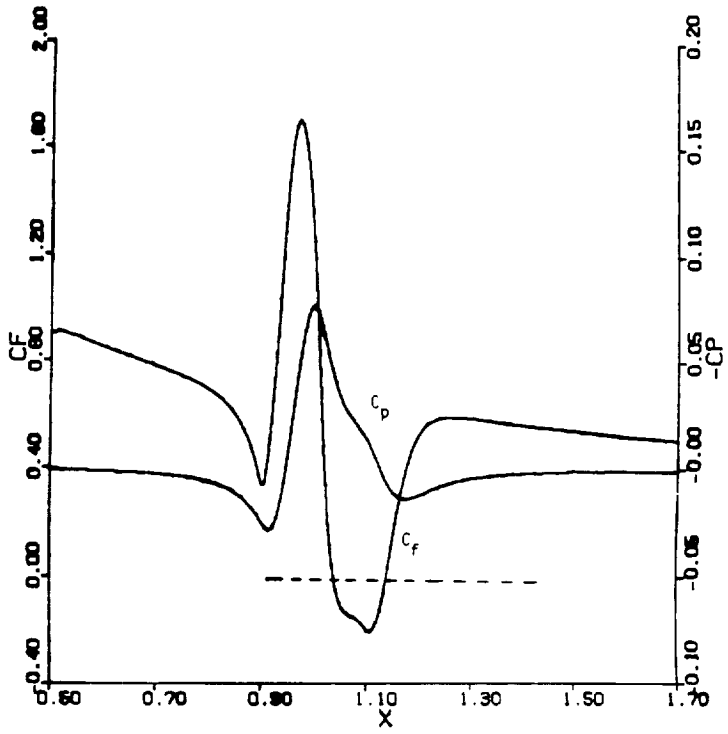

Figure 3. Distributions of (a) skin friction coefficient $c_f\sqrt{Re}$, and (b) pressure coefficient c_p for $h = 3$, $Re = 10^6$; small separation bubble.

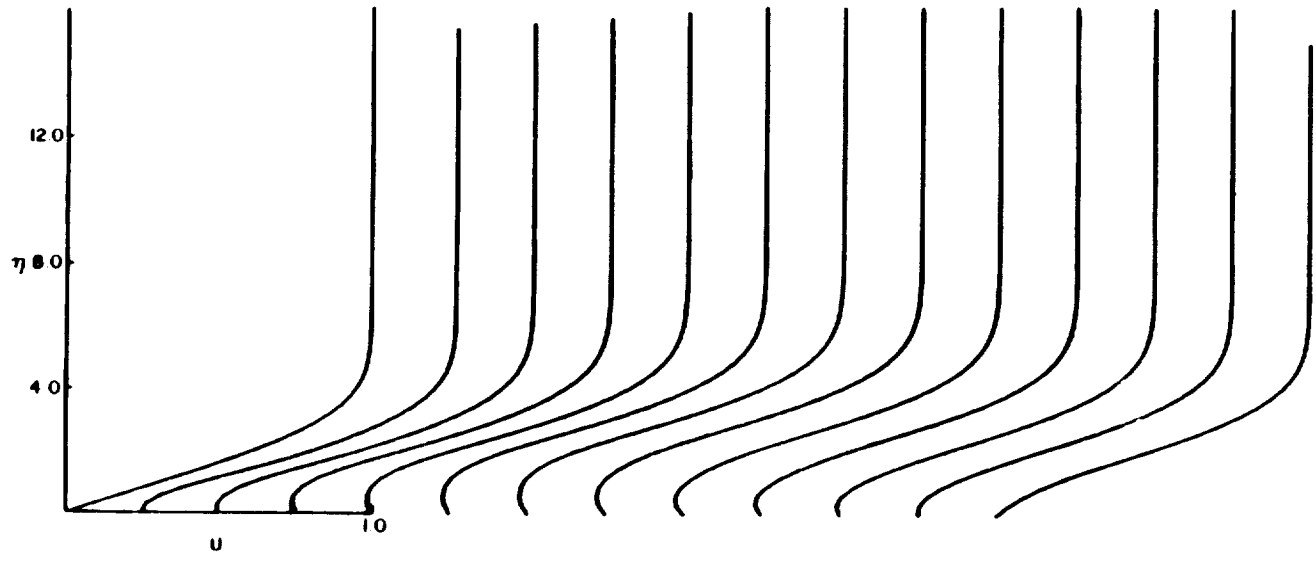

Figure 4. Variation of streamwise velocity profiles along the plate for hump No. 14 in Table 1. The hump is centered at $X_m^*/L^* = 1.0(R = 983)$, $h^*/b^* = 0.031$, $b^*/L^* = 0.1$.

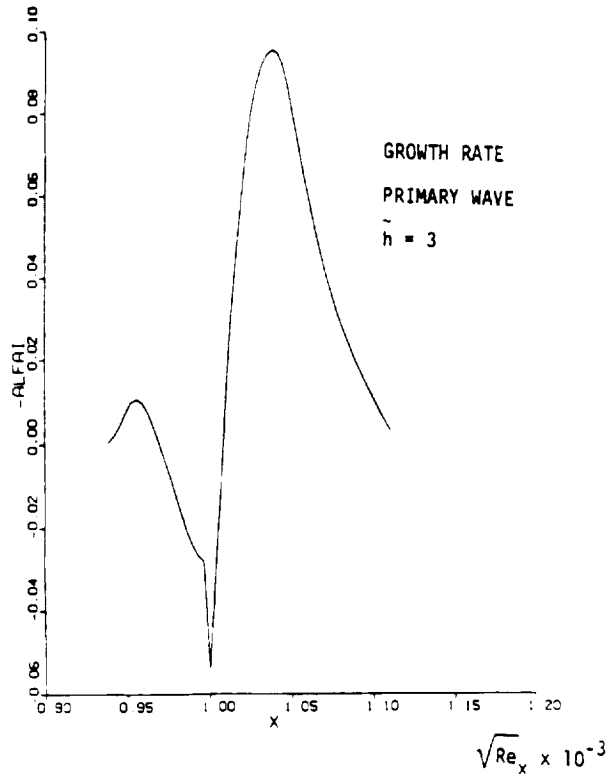

Figure 5. Variation of the growth rate with streamwise position.

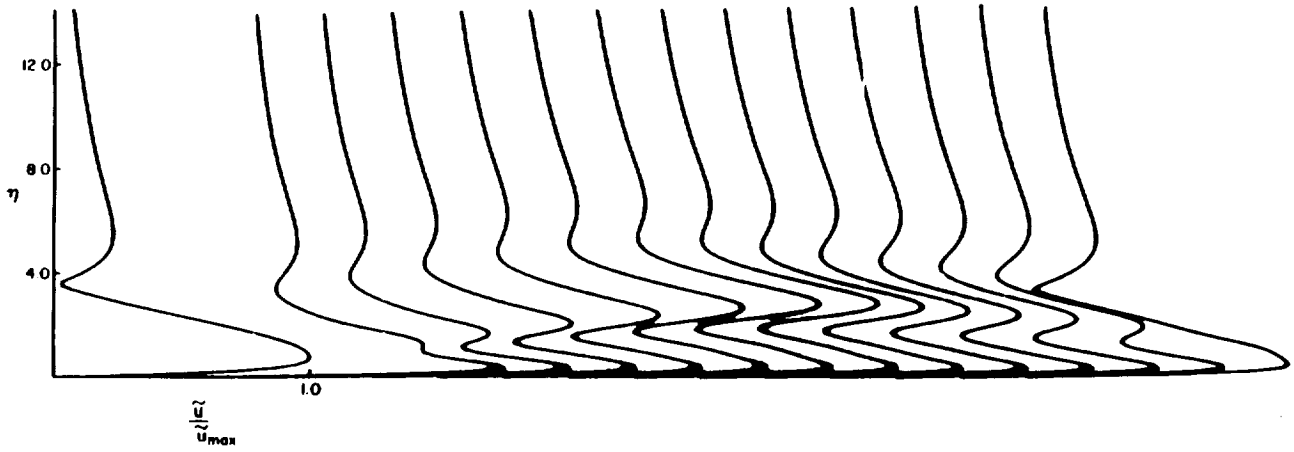

Figure 6. Variation of the eigenfunction of hump No. 14 in Table 1 along the plate at frequency $F = 55 \times 10^{-6}$.

Report Documentation Page

1. Report No.	2. Government Accession No.	3. Recipient's Catalog No.
NASA CP-2487, Part 1		

4. Title and Subtitle	5. Report Date
Research in Natural Laminar Flow and Laminar-Flow Control	December 1987
	6. Performing Organization Code

7. Author(s)	8. Performing Organization Report No.
Jerry N. Hefner and Frances E. Sabo, Compilers	L-16350
	10. Work Unit No. 505-60-31-06

9. Performing Organization Name and Address	11. Contract or Grant No.
NASA Langley Research Center Hampton, VA 23665-5225	
	13. Type of Report and Period Covered Conference Publication
12. Sponsoring Agency Name and Address	14. Sponsoring Agency Code
National Aeronautics and Space Administration Washington, DC 20546-0001	

15. Supplementary Notes

16. Abstract

Since the mid 1970's, NASA, industry, and universities have worked together to conduct important research focused at developing laminar-flow technology that could reduce fuel consumption for general aviation, commuter, and transport aircraft by as much as 40 to 50 percent. This research, which was initiated under the NASA Aircraft Energy Efficiency Program and continued through the Research and Technology Base Program, has proved very successful with many very significant and impressive results having been obtained.

This symposium was planned in view of the recent accomplishments within the areas of laminar-flow control and natural laminar flow, and the potential benefits of laminar-flow technology to the civil and military aircraft communities in the United States. The symposium included technical sessions on advanced theory and design tool development, wind tunnel and flight research, transition measurement and detection techniques, low and high Reynolds number research, and subsonic and supersonic research.

17. Key Words (Suggested by Author(s))	18. Distribution Statement
Laminar flow Natural laminar flow Aerodynamics	[redacted] Subject Category 02

19. Security Classif. (of this report)	20. Security Classif. (of this page)	21. No. of pages	22. Price
Unclassified	Unclassified	329	

[redacted]

NASA-Langley, 1987